Journal of Solid State Chemistry 187 (2012) 172–176

Contents lists available at SciVerse ScienceDirect

Journal of Solid State Chemistry

journal homepage: www.elsevier.com/locate/jssc

Why $MnIn_2O_4$ spinel is not a transparent conducting oxide?

M.J. Martínez-Lope [a], M. Retuerto [a,b], C. de la Calle [a], Florence Porcher [c], J.A. Alonso [a,*]

[a] Instituto de Ciencia de Materiales de Madrid, C.S.I.C., Cantoblanco E-28049 Madrid, Spain
[b] Department of Chemistry, Rutgers State University of New Jersey, Piscataway, NJ 08854-8087, USA
[c] Laboratoire Leon Brillouin, CEA/Saclay, 91191 Gif Sur Ivette Cedex, France.

ARTICLE INFO

Article history:
Received 1 September 2011
Received in revised form
14 December 2011
Accepted 4 January 2012
Available online 13 January 2012

Keywords:
Indium spinel
In_2MnO_4
TCO
Mn mixed valence
Inversion degree

ABSTRACT

The title compound has been synthesized by a citrate technique. The crystal structure has been investigated at room temperature from high-resolution neutron powder diffraction (NPD) data. It crystallizes in a cubic spinel structure, space group $Fd\bar{3}m$, $Z=8$, with $a=9.0008(1)$ Å at 295 K. It exhibits a crystallographic formula $(Mn_{0.924(2)}In_{0.076(2)})_{8a}(In_{1.804(2)}Mn_{0.196(2)})_{16d}O_4$, where 8a and 16d stand for the tetrahedral and octahedral sites of the spinel structure, respectively, with a slight degree of inversion, $\lambda=0.08$. $MnIn_2O_4$ shows antiferromagnetic interactions below $T_N \approx 40$ K, due to the statistical distribution of Mn ions over the two available sites. Unlike the related $MgIn_2O_4$ and $CdIn_2O_4$ spinels, well known as transparent conducting oxides, $MnIn_2O_4$ is not transparent and shows a poor conductivity ($\sigma=0.38$ S cm^{-1} at 1123 K): the presence of Mn ions, able to adopt mixed valence states, localizes the charges that, otherwise, would be delocalized in the spinel conduction band.

1. Introduction

A few semiconducting oxides have been described to be simultaneously transparent and highly conductive. Transparent conducting oxides (TCOs) have widespread uses in photoelectrochemistry, as electrodes in solar cells and liquid crystal displays, heat-reflecting window coatings and windshield defrosters. The commercial transparent-conducting oxide of choice is ITO (tin-doped indium oxide, $In_{2-x}Sn_xO_3$). ITO has a typical conductivity of $1–5 \times 10^3$ S cm^{-1} and a transparency of 85–90% in thin films [1]. However, some ternary oxides containing Sn or In can also be transparent and highly conductive [2]. These include Cd_2SnO_4 [2–5], $MgIn_2O_4$ [6,7], $CdIn_2O_4$ [2,8,9], In_2TeO_6 [2,10], and $CdSnO_3$ [2,11,12]. In the absence of ions able to adopt mixed valence states, electrons are generally assumed to be introduced by oxygen deficiency.

Among them, $MgIn_2O_4$ and $CdIn_2O_4$ exhibit a spinel structure. The structural characteristics of spinels are advantageous for producing TCOs [13], in particular the easiness of formation of extended conduction bands, which is prerequisite for n-type TCOs containing cations with $d^{10}s^0$ electronic configuration, such as In^{3+}. However, the number of indium-containing spinels is scarce. $MgIn_2O_4$ [7] presents an inverse spinel structure and it has been adopted as the transparent material of choice in optoelectronic device fabrication due to its high optical transparency and electrical conductivity. It is a very promising material as a transparent electronic conductor. It shows a wide optical band gap of approximately 3.4 eV, even wider than that of ITO. Electrical conductivity of the sintered sample of $MgIn_2O_4$ at room temperature has reached almost 10^2 S cm^{-1} with no intentional doping. The conduction was found to be due to electrons introduced from oxygen vacancies. A second example of indium-containing spinels is $CdIn_2O_4$. It is also an inverse spinel with $a=9.1673(5)$ Å [2], better written as $In(CdIn)O_4$; it exhibits a conductivity of 2 10^3 S cm^{-1}. Also, a substantial solid solubility of In_2O_3 in the spinel Zn_2SnO_4 ($Zn_{2-x}Sn_{1-x}In_xO_{4-d}$, $x=0$ to 0.45) was discovered [14]. The reduced material showed improved conductivity at higher In contents.

In this paper we describe the structure and properties of an indium-containing spinel-type oxide of stoichiometry $MnIn_2O_4$. In contrast with $MgIn_2O_4$ and $CdIn_2O_4$ it does not show the characteristic features of TCO's. A neutron powder diffraction, carried out to determine its crystallographic features, such as the inversion degree [15] (thanks to the contrast between In and Mn scattering lengths for neutrons) and bond valence of the involved cations, was useful to understand the physical properties of this material. Also, the electrical properties are described.

2. Experimental

$MnIn_2O_4$ spinel was prepared as a brown polycrystalline powder from citrate precursors obtained by a soft chemistry procedure. Stoichiometric amounts of analytical grade In_2O_3 and $MnCO_3$ were dissolved in citric acid, by adding several droplets of concentrated HNO_3 to favor the solution of indium oxide.

* Corresponding author. Fax: +34 91 372 06 23.
E-mail address: ja.alonso@icmm.csic.es (J.A. Alonso).

0022-4596/$ - see front matter © 2012 Elsevier Inc. All rights reserved.
doi:10.1016/j.jssc.2012.01.009

The mixture of citrate and nitrate solutions was slowly evaporated, leading to organic resins where a random distribution of the involved cations is expected at an atomic level. This resin was first dried at 393 K, the sample was then heated at 873 K for 12 h in air in order to eliminate all the organic materials and nitrates. This treatment gave rise to highly reactive precursor materials. The precursor was treated at 1473 K for 12 h and then 1673 K for 12 h in a N_2 flow, with intermediate grinding. The treatment in inert atmosphere is essential to stabilize divalent and/or trivalent Mn ions in the spinel structure, otherwise mixtures of Mn oxides and In_2O_3 are obtained in air atmosphere.

The initial characterization of the product was carried out by laboratory x-ray diffraction in a Bruker-axs D8 diffractometer (40 kV, 30 mA), controlled by a DIFFRACT^{plus} software, in Bragg–Brentano reflection geometry with CuK_α radiation ($\lambda=1.5418$ Å) and a PSD detector. The data were obtained between 10 and 100° 2θ in steps of 0.05°. Neutron powder diffraction (NPD) data were collected in the 3T2 high-resolution diffractometer ($\lambda=1.2252$ Å) at the Laboratoire Léon Brillouin in Saclay (France). About 4 g of sample were placed in a vanadium can; the counting time was 12 h. The refinement of the crystal structure was performed by the Rietveld method using the Fullprof code [16]. The peaks profiles were fitted by the Thompson–Cox–Hastings pseudo-Voigt function corrected for axial divergence asymmetry. The following parameters were refined in the final run of the fit: scale factor, background coefficients, zero-point error, unit-cell parameters, pseudo-Voigt corrected for asymmetry parameters, positional coordinates, isotropic displacement factors, anti-site disordering, and occupancy factors for indium and manganese atoms. The coherent scattering lengths for In, Mn, and O were 4.065, −3.74 and 5.803 fm, respectively.

The magnetic measurements were performed in a commercial SQUID magnetometer from Quantum Design. The *dc* magnetic susceptibility was measured in the temperature interval $1.8<T<300$ K, under a magnetic field of 1 kOe. As regarding the isothermal magnetization curves, different hysteresis cycles were obtained at $T=5$ and 300 K and for a magnetic field ranging from −50 kOe to 50 kOe.

The electronic conductivity was measured by the conventional four-probe technique in a bar-shaped pellet of dimensions $10\times3\times3$ mm^3, sintered at the synthesis temperature for 4 h. The measurements were carried out in the temperature range 673–1123 K in N_2 flow.

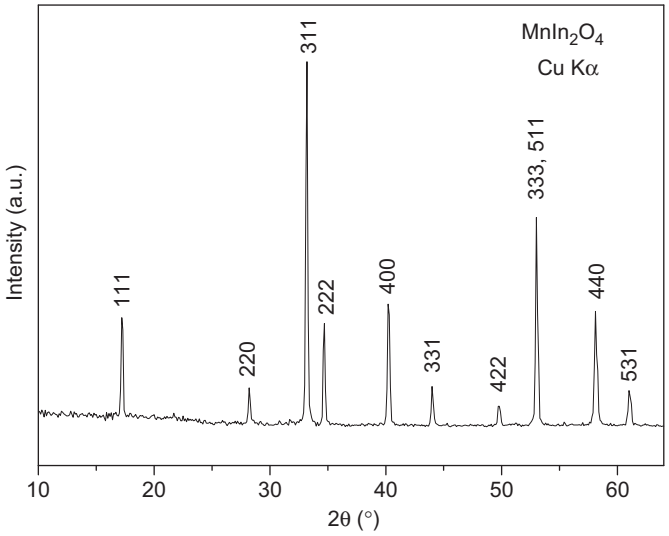

Fig. 1. XRD pattern $MnIn_2O_4$, indexed in a face-centered cubic unit cell with $a=9.0008(1)$ Å.

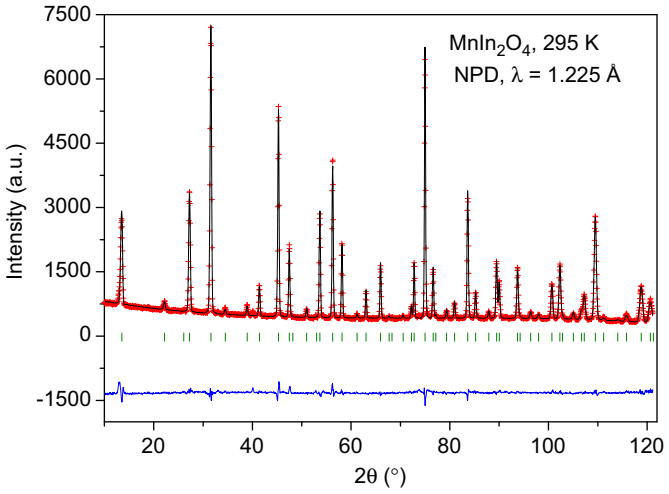

Fig. 2. Observed (crosses), calculated (full line), and difference (bottom) Rietveld profiles for $MnIn_2O_4$ at 295 K from NPD data.

3. Results

$MnIn_2O_4$ was obtained as well-crystallized powder. The XRD diagram is shown in Fig. 1. The pattern is characteristic of a single-phase spinel oxide and it can be indexed in a cubic lattice in the space group $Fd\bar{3}m$, with unit cell parameter $a=9.0008(1)$ Å. This pattern corresponds to the JCPDS file no. 40-1401, given for the In_2MnO_4 oxide [17], with $a=9.000$ Å.

3.1. Structural refinement

The refinement of the crystal structure of $MnIn_2O_4$ was performed from NPD data obtained at room temperature with a $\lambda=1.2252$ Å wavelength. The structure was defined in the cubic space group $Fd\bar{3}m$ (No. 227), origin at center ($\bar{3}m$). In a first approach, Mn and In atoms were located at the 8a (1/8,1/8,1/8) and 16d (1/2,1/2,1/2) crystallographic Wyckoff sites, respectively, and oxygen atoms at 32e (u,u,u) positions. The variable parameter for the oxygen position, $u=0.25927(3)$, is close to that expected ($u=0.25$) for normal spinels [15]. Antisite disordering considering that some Mn could occupy the octahedral 16*d* sites and some In the tetrahedral 8*a* positions was refined, reaching $R_{Bragg}=5\%$. An extra reduction of the discrepancy Bragg factor down to 3.69% was gained in the final refinement by unconstraining the indium and manganese occupancy factors at each site, allowing a slight deviation from the nominal 2:1 stoichiometry. A further refinement of the occupancy factor of the oxygen atoms led to a full oxygen stoichiometry within the standard deviations. The final crystallographic formula is $(Mn_{0.924(2)}In_{0.076(2)})_{8a}(In_{1.804(2)}Mn_{0.196(2)})_{16d}O_{4.00(2)}$. This means a global stoichiometry $Mn_{1.12}In_{1.88}O_4$, slightly In-defective, probably due to some In evaporation in the synthesis process at 1673 K. Assuming a trivalent state for In, the average Mn oxidation state is 2.11+. An excellent fit was obtained for this model, as shown in Fig. 2. The most important structural parameters of the crystal structure at RT and the discrepancy factors after the refinements are listed in Table 1. Table 2 contains the main interatomic distances and angles. A view of the crystal structure of $MnIn_2O_4$ is illustrated in Fig. 3.

3.2. Magnetic and electrical measurements

Fig. 4 displays the *dc* susceptibility curve of $MnIn_2O_4$. The susceptibility smoothly increases upon cooling; below 40 K a very slight change in the slope of the curve is observed, which could be

Table 1
Unit-cell, positional, displacement B parameters and site occupancies for $MnIn_2O_4$, refined in the cubic $Fd\bar{3}m$ space group (No. 227), origin at center ($\bar{3}m$), from NPD data at 295 K. Unit-cell parameter $a=9.0008(1)$ Å.

Atom	Site	X	y	z	B (Å^2)	f_{occ}
In1	8a	1/8	1/8	1/8	0.34(3)	0.076(2)
Mn1	8a	1/8	1/8	1/8	0.34(3)	0.924(2)
In2	16d	1/2	1/2	1/2	0.13(1)	0.902(1)
Mn2	16d	1/2	1/2	1/2	0.13(1)	0.098(1)
O	32e	0.25927(3)	0.25927(3)	0.25927(3)	0.411(5)	1.001(5)
Reliability factors	R_p	R_{wp}	R_{exp}	χ^2	R_{Bragg}	
	2.94(%)	3.88(%)	1.84(%)	4.46	3.69(%)	

Table 2
Main interatomic distances (Å) and angles (°) in the $MnIn_2O_4$ spinel, refined at 295 K from NPD data.

$(Mn,In)O_4$ tetrahedra				
(Mn1,In1)O	×4	2.0932(4)	O-(Mn1,In1)-O	109.47
			(Mn1,In1)-O-(In2,Mn2)	122.15(1)
(In2,Mn2)-O octahedra				
(In2,Mn2)-O	×6	2.1700(6)	O-(In2,Mn2)-O	94.49(2)
			O-(In2,Mn2)-O	85.51(2)
			(In2,Mn2)-O-(In2,Mn2)	94.32(1)

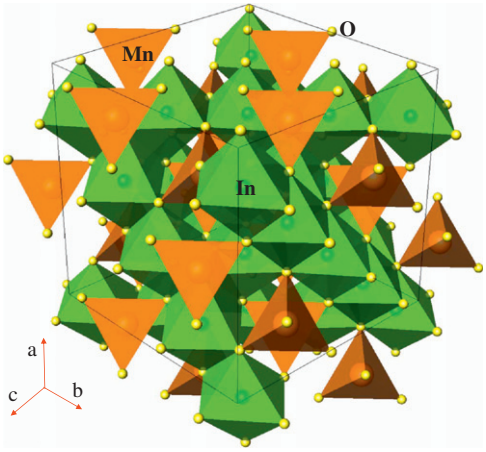

Fig. 3. View of the crystal structure of $MnIn_2O_4$, approximately along the [1 1 1] direction, showing the intercrossed chains of InO_6 octahedra sharing edges, running along [1 1 0] directions.

related to weak magnetic interactions. The reciprocal susceptibility data (inset of Fig. 4) can be fitted to a Curie–Weiss law above 100 K, giving a paramagnetic temperature of $\Theta_{Weiss}=-91.82(1)$ K, also suggesting the presence of weak antiferromagnetic interactions. The value of the effective paramagnetic moment is $\mu_{eff}=5.60(2)\ \mu_B$/f.u. The theoretical effective magnetic moment of this material was determined using the equation $\mu_{eff}=(\Sigma n_i\mu_i^2)^{1/2}$ applied to the formula determined from NPD data, $Mn^{2+}_{1.00}Mn^{3+}_{0.12}In_{1.88}O_4$, containing mixed Mn^{2+} and Mn^{3+} ions (with average nominal oxidation state of 2.11+). The effective magnetic moments in the ground state for Mn^{3+} (high spin: 4.90 μ_B), Mn^{2+} (5.92 μ_B) were considered. The calculated effective magnetic moment is 6.16 μ_B, in reasonable agreement with the experimental value.

In the isothermal magnetization curves displayed in Fig. 5, a slight curvature and a very narrow hysteresis loop (coercive field = 160 Oe) is observed at $T=5$ K with a maximum magnetization of 0.5 μ_B/f.u. reached for the maximum applied field of 50 K Oe. At 300 K the isothermal magnetization curve presents a linear behavior characteristic of a paramagnetic state.

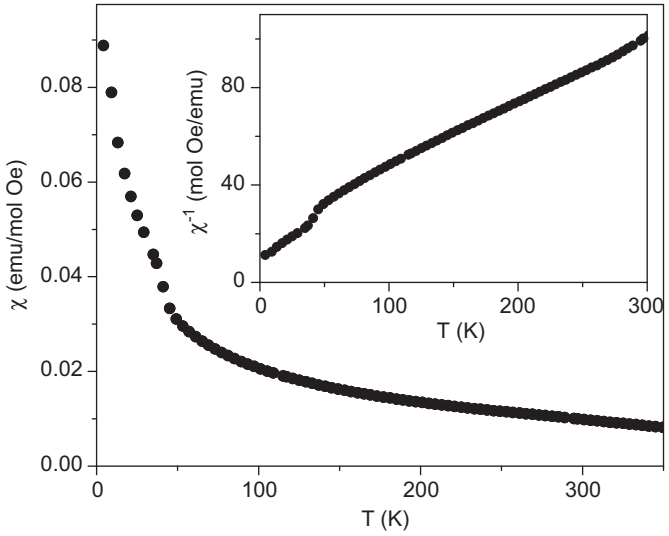

Fig. 4. Temperature variation of the magnetic susceptibility for $MnIn_2O_4$. The inset shows the reciprocal susceptibility, and the Curie–Weiss linear fit.

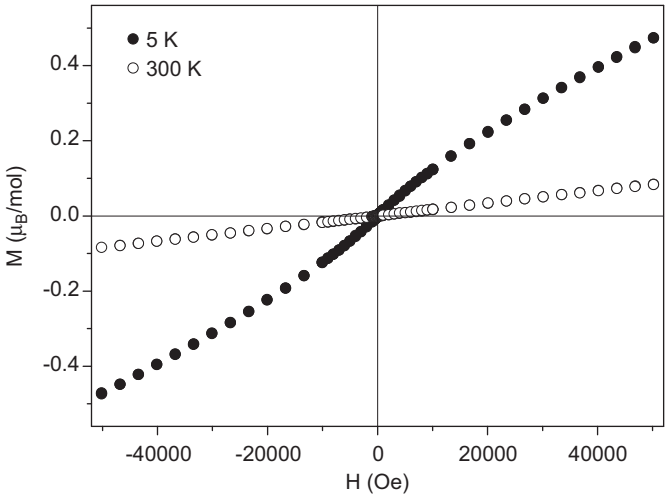

Fig. 5. Isothermal magnetization vs. magnetic field cycle at $T=5$ K and 300 K.

The temperature dependence of the electrical conductivity in the 873–1123 K range is shown in Fig. 6(a). A semiconducting behavior characterized by a positive slope is observed in all the temperature range; a maximum conductivity of $\sigma\approx 0.38$ S cm^{-1} is measured at 1123 K. A variable range hopping mechanism where $\sigma=\sigma_0.\exp(-T_0/T)^{1/4}$ is successfully used to fit the conductivity data, with $R=0.988$, as shown in Fig. 6(b).

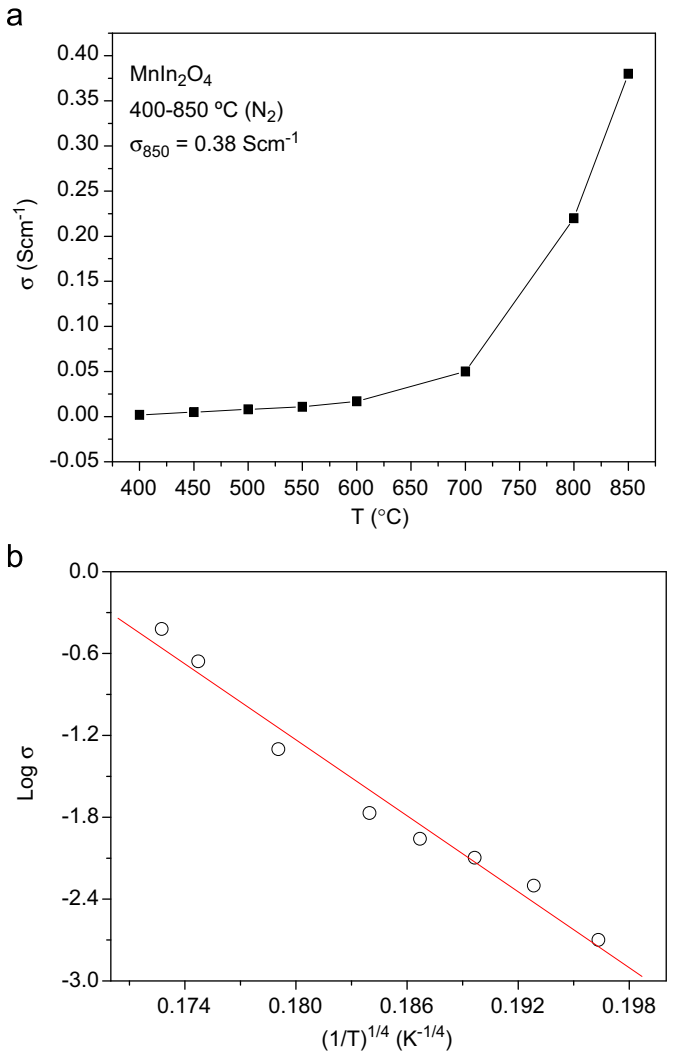

Fig. 6. (a) Electrical conductivity vs. temperature and (b) fit to a variable-range hopping law for the high-temperature regime.

4. Discussion

The refinement of the crystal structure of the $MnIn_2O_4$ spinel in the cubic $Fd\bar{3}m$ space group shows a small degree of inversion; if we define it as the proportion of In at tetrahedral sites, $\lambda=0.08$. It can be considered, therefore, as a normal spinel, in contrast, for instance with $CdIn_2O_4$, which is an inverse spinel [2]. On the other hand, the unconstrained refinement of the In/Mn occupancy factors at 8a and 16d sites leads to a slight deviation from the nominal stoichiometry. We can assume a valence distribution as $(Mn^{2+}_{0.924(2)}In_{0.076(2)})_{8a}(In_{1.804(2)}Mn^{2.61+}_{0.196(2)})_{16d}O_4$, where Mn^{2+} ions occupy the tetrahedral 8*a* sites, whereas 61% of Mn^{3+} and 39% Mn^{2+} are located at the octahedral positions. In many Mn-containing spinels Mn^{2+} ion are located at tetrahedral 8a sites, as observed in the normal Mn_3O_4 (or $MnMn_2O_4$) spinel. Although Mn_3O_4 (Hausmannite) is tetragonal, space group $I4_1/amd$, the cationic distribution is clearly as stated [18]. However, there are examples of inverse spinels containing Mn^{2+} at octahedral positions; typically, $MnFe_2O_4$ has a degree of inversion of $\lambda=0.20$ [19,20] corresponding to 20% Mn^{2+} at 16d sites.

As shown in Table 2, Mn_1 at 8a sites is fourfold coordinated within regular tetrahedral units, with Mn_1–O distances 2.0932(4) Å, in good agreement with the ionic-radii sum [21] for $^{IV}Mn^{2+}$ (0.66 Å) and $^{IV}O^{2-}$ (1.40 Å) of 2.06 Å. In the same way, the In_2–O bond-lengths in the octahedral units 2.1700(6) Å are close to those expected for $^{VI}In^{3+}$ (0.80 Å) of 2.20 Å. The anti-site disordering of In at Mn sites account for the observed discrepancies. Moreover, the calculation of the bond-valences [22–24] for Mn at 8a and In at 16d sites are in close agreement with the nominal valences, +1.904(1) and +3.143(1), respectively. In the Brown's model [22] the valence is the sum of the individual bond valences (s_i) for Mn–O and In–O bonds. Bond valences are calculated as $s_i=\exp[(r_0-r_i)/B]$; $B=0.37$, $r_0=1.790$ for the Mn^{2+}–O^{2-} pair and $r_0=1.902$ for the In^{3+}–O^{2-} pair, from [23]. Individual Mn–O and In–O distances (r_i) are taken from Table 2.

As shown in Fig. 3, the spinel structure contains inter-crossed chains of edge-sharing octahedra running along ⟨1 1 0⟩ directions. Along these chains the resulting short cation–cation distance enhances the direct overlap of vacant *s* orbitals between neighboring cations and the formation of an extended conduction band. In this respect, the linear chains have been defined as "highways" for electrons [13]. An electron-doping effect, which may result from the presence of oxide-ion vacancies, can thus lead to an impressive conductivity by partially filling with free electrons this extended conduction band. This is the mechanism playing in $MgIn_2O_4$ and $CdIn_2O_4$, both exhibiting a surprisingly high conductivity. However, in the present $MnIn_2O_4$ spinel we determined a rather poor conductivity, lower than 0.38 S cm^{-1}. The difference is clearly the presence of Mn ions, able to adopt mixed valence states and, therefore, to localize the charges that otherwise, would be delocalized in the mentioned conduction band. In other words, the variability of the oxidation states of Mn at the octahedral positions (10%) immediately cancels any electron-doping effect resulting from the presence of any oxide-ion vacancies, thus emptying the conduction band and dramatically reducing the electronic conductivity. Also, the presence of mixed-valence Mn^{2+} and Mn^{3+} provides the characteristic brown color, disturbing the transparency of this oxide.

The susceptibility vs. temperature curve of $MnIn_2O_4$ displays antiferromagnetic interactions below $T_N\approx 40$ K. Given that we are in the presence of a normal spinel, with most of the Mn ions occupying the tetrahedral positions, it is reasonable to think that the magnetic interactions are weak since there are no direct Mn–O–Mn superexchange paths, excepting those occurring because of the random distribution of some (10%) Mn ions over the octahedral sites. It is important to remember that the MnO_4 tetrahedra constitute isolated magnetic units in the structure, linked to four non-magnetic InO_6 octahedra each, excepting those MnO_6 octahedra due to the slight antisite disordering.

The curves of the magnetization vs. field show a slight curvature at 5 K. We believe this is due to subtle Mn_{8a}–O–Mn_{16d} interactions due to the anti-site disordering, as commented above. As it is well known, in other related spinel compounds like the ferrites $MnFe_2O_4$ the presence of magnetic cations at both tetrahedral and octahedral sites produces a large magnetic response; in these ferrimagnetic materials the magnetic cations are ordered over both positions (Fe at octahedral sites and Mn in tetrahedral coordination). In the present In spinel the subtle magnetic response observed in the 5 K isotherm is reminiscent of the ferrimagnetic behavior observed, for instance, in the Mn_3O_4 spinel (also containing Mn^{2+} at tetrahedral sites and Mn^{3+} at octahedral positions). According to literature, this spinel is ferrimagnetic below 42.5 K [25] to 46 K [26]; it is plausible that the present compound develops Mn_{8a}–O–Mn_{16d} magnetic interactions with similar strength, giving rise to a subtle ferrimagnetism phenomenon below a given temperature ($T_C=40$ K), probably lacking from long-range coherence.

5. Conclusions

$MnIn_2O_4$ crystallizes in the spinel structure, as demonstrated from a high-resolution NPD analysis. There is a slight degree of

inversion, with 8% of In at the tetrahedral sites; otherwise Mn^{2+} ions are located at these positions. The edge-sharing octahedra contain a statistical distribution of 90% In^{3+} and 10% Mn^{3+} cations. The conductivity of this spinel is several orders of magnitude lower than those of $MgIn_2O_4$ or $CdIn_2O_4$: the variability of the oxidation states of Mn at the octahedral positions (10%) immediately cancels any electron-doping effect resulting from the presence of any oxide-ion vacancies, thus emptying the conduction band of mobile charge carriers.The magnetic measurements show a Curie–Weiss behavior with an effective paramagnetic moment confirming the determined charge distribution. The spinel displays antiferromagnetic interactions below $T_N \approx 40$ K, probably driven by Mn_{8a}–O–Mn_{16d} magnetic couplings generated as a consequence of the statistical occupancy of Mn over the two available positions; the slight curvature observed in the magnetization isotherms is reminiscent of the ferrimagnetic behavior described for Mn_3O_4 Hausmannite.

Acknowledgments

We thank the financial support of the Spanish Ministry of science and Innovation to the project MAT2010–16404. This work was partially performed at the Orphé reactor, Laboratoire Léon Brillouin, Saclay, France. We are grateful to Dr. Espinosa for performing the magnetic measurements.

References

[1] N.R. Lyman, Proceedings of the symposium on electrochromic materials, Electrochem. Soc. Proc. 90 (2) (1990) 201.
[2] R.D. Shannon, J.L. Gillson, R.J. Bouchard, J. Phys. Chem. Solids 38 (1977) 877–881.
[3] R. Mamazza, D.L. Morel, C.S. Ferekides, Thin Solid Films 484 (2005) 26–33.
[4] A.W. Metz, M.A. Lane, R. Kannewurf, K.R. Poepelmeier, T.J. Marks, Chem. Vap. Deposition 10 (2004) 297–300.
[5] E. Leja, K. Budzyńska, T. Pisarkiewicz, T. Stapiński, Thin Solid Films 100 (1983) 203–208.
[6] S.E. Dali, M. Jayachandran, M.J. Chockalingam, J. Mat. Sci. Lett. 18 (1999) 915–917.
[7] N. Ueda, T. Omata, N. Hikuma, K. Ueda, H. Mizoguchi, T. Hashimoto, H. Kawazoe, Appl. Phys. Lett. 61 (1992) 1954–1955.
[8] F.P. Koffyberg, F.A. Benko, Appl. Phys. Lett. 37 (1980) 320–322.
[9] B. Li, L. Zeng, F. Zhang, Phys. Status Solidi 201 (2004) 960–966.
[10] B. Shemirani, F.P. Koffyberg, Mat. Res. Bull. 27 (1992) 693–698.
[11] X-H Wu, Y.-D Wang, Y.-F Li, Z.-L Zhou, Mat. Chem. Phys. 77 (2002) 588–593.
[12] G. Natu, Y. Wu, J. Phys. Chem. C 114 (2010) 6802–6807.
[13] H. Kawazoe, K. Ueda, J. Am. Ceram. Soc. 82 (1999) 3330–3336.
[14] G.B. Palmer, K.R. Poeppelmeier, T.O. Mason, J. Sol. State Chem. 134 (1997) 192–197.
[15] R.W.G. Wyckoff, Crystal Structures, Wiley Interscience, New York, 1964.
[16] J. Rodriguez-Carvajal, Physica B 192 (1993) 55–69.
[17] N. Kimizuka, T. Mohri, J. Solid State Chem. 78 (1989) 98–107.
[18] V. Baron, J. Gutzmer, H. Rundloef, R. Tellgren, Am. Mineral. 83 (1998) 786–793.
[19] J. Wang, Y. Wu, Y. Zhu, Y, Int. J. Mod. Phys. B 21 (2007) 723–730.
[20] E. Kravtsov, D. Haskel, A. Cady, A. Yang, C. Vittoria, X. Zuo, V.G. Harris, Phys. Rev. B 74 (2006) 104114.
[21] R.D. Shannon, Acta Crystallogr. A32 (1976) 751–767.
[22] I.D. Brown, in: M. O'Keefe, A. Navrotsky (Eds.), Structure and Bonding in Crystals, Academic Press, New York, 1981.
[23] N.E. Brese, M. O'Keefe, Acta Crystallogr. Sect. B 47 (1991) 192–197.
[24] I.D. Brown, Z. Kristallogr. 199 (1992) 255–267.
[25] B. Boucher, R. Buhl, M. Perrin, J. Phys. Chem. Solids 32 (1971) 2429–2437.
[26] D.E. Cox, G. Shirane, R.J. Birgeneau, J.B. McChesney, Phys. Rev. 188 (1969) 930–932.